JOURNAL OF GEOPHYSICAL RESEARCH, VOL. 103, NO. D16, PAGES 19,673–19,689, AUGUST 27, 1998

Raman lidar measurements of aerosol extinction and backscattering
2. Derivation of aerosol real refractive index, single-scattering albedo, and humidification factor using Raman lidar and aircraft size distribution measurements

R.A. Ferrare,[1,2] S.H. Melfi,[3] D.N. Whiteman,[4] K.D. Evans[5], M. Poellot,[6] and Y.J. Kaufman[4]

Abstract. Aerosol backscattering and extinction profiles measured by the NASA Goddard Space Flight Center Scanning Raman Lidar (SRL) during the remote cloud sensing (RCS) intensive operations period (IOP) at the Department of Energy Atmospheric Radiation Measurement (ARM) southern Great Plains (SGP) site during two nights in April 1994 are discussed. These profiles are shown to be consistent with the simultaneous aerosol size distribution measurements made by a PCASP (Passive Cavity Aerosol Spectrometer Probe) optical particle counter flown on the University of North Dakota Citation aircraft. We describe a technique which uses both lidar and PCASP measurements to derive the dependence of particle size on relative humidity, the aerosol real refractive index n, and estimate the effective single-scattering albedo ω_0. Values of n ranged between 1.4–1.5 (dry) and 1.37–1.47 (wet); ω_0 varied between 0.7 and 1.0. The single-scattering albedo derived from this technique is sensitive to the manner in which absorbing particles are represented in the aerosol mixture; representing the absorbing particles as an internal mixture rather than the external mixture assumed here results in generally higher values of ω_0. The lidar measurements indicate that the change in particle size with relative humidity as measured by the PCASP can be represented in the form discussed by *Hanel* [1976] with the exponent $\gamma = 0.3 \pm 0.05$. The variations in aerosol optical and physical characteristics captured in the lidar and aircraft size distribution measurements are discussed in the context of the meteorological conditions observed during the experiment.

1. Introduction

Accurate aerosol measurements are required for understanding shortwave (visible) radiative transfer since aerosols affect the Earth's climate by scattering and absorbing solar radiation (direct effect) and by altering the scattering, absorption, lifetime, and extent of clouds (indirect effect). By reflecting solar radiation, atmospheric aerosols may reduce the warming associated with increases in greenhouse gases [*Charlson et al.*, 1992; *Intergovernmental Panel on Climate Change (IPCC)*, 1994] although the magnitude of the aerosol direct radiative cooling effect may be small [*Kiehl and Briegleb*, 1993; *IPCC*, 1995]. In fact, depending on the composition and vertical distribution of aerosols and the surface albedo, aerosols may actually raise rather than lower surface temperatures [*Hansen et al.*, 1997]. Changes in the number density, size distribution, and composition of aerosols can affect the number and sizes of cloud drops and can consequently affect the cloud albedo [*Twomey*, 1977]. Indeed, by controlling cloud microphysics, atmospheric aerosols play an important role in the atmospheric water cycle [*Twomey*, 1991].

Because meteorological parameters such as temperature, humidity, and wind speed affect aerosol physical and optical properties [*Fenn et al.*, 1981; *Nilsson et al.*, 1982], it is important to study aerosols in their natural state. Surface-based in situ measurements provide detailed information on aerosol physical and optical properties [*Nilsson et al.*, 1982; *Rood et al.*, 1985] but cannot ascertain these properties as a function of altitude. Aircraft instruments can measure aerosol properties at selected altitudes but not simultaneously. Aircraft in situ measurements also often subject the aerosols to changes in relative humidity between the atmosphere and the instrument [*Baumgardner and Huebert*, 1993]. The aerosol collection efficiency depends on size and therefore may not represent all sizes of particles correctly [*Huebert et al.*, 1990]. Passive measurements of solar transmission and sky radiation have been used extensively to measure the aerosol size distribution and phase function [*King et al.*, 1978; *Nakajima et al.*, 1983; *Shiobara et al.*, 1991;

[1]Hughes STX, NASA Goddard Space Flight Center, Greenbelt, Maryland.
[2]Now at NASA Langley Research Center, Hampton, Virginia.
[3]Department of Physics, University of Maryland, Baltimore, Maryland.
[4]NASA Goddard Space Flight Center, Greenbelt, Maryland.
[5]Joint Center for Earth Systems Technology, University of Maryland, Baltimore, Maryland.
[6]Department of Atmospheric Sciences, University of North Dakota, Grand Forks, North Dakota.

Paper number 98JD01647.
0148-0227/98/98JD-01647$09.00

Wendisch and von Hoyningen-Huene, 1992; *Kaufman et al.*, 1994]. These measurements are averaged over an entire atmospheric column and cannot provide information regarding the vertical distribution of aerosols.

In part 1, *Ferrare et al.* [this issue] showed how the GSFC Scanning Raman Lidar can be used to remotely measure vertical profiles of aerosol extinction and backscattering. A detailed description was given of the NASA GSFC Scanning Raman Lidar nighttime measurements of aerosol backscattering and extinction profiles. The methods used to derive these profiles were described, and the lidar measurements were compared with nephelometer measurements of aerosol scattering and Sun photometer measurements of aerosol optical thickness acquired during the remote cloud study (RCS) intensive operations period (IOP) held in April 1994 at the Department of Energy (DOE) atmospheric radiation measurement (ARM) southern Great Plains (SGP) site. In this part 2 paper, we first use Mie theory to show how variations in relative humidity, refractive index, and single-scattering albedo affect the lidar measurements of aerosol backscattering and extinction. Next, we describe and demonstrate a technique which uses a combination of the SRL measurements of aerosol extinction and backscattering with the aerosol size distributions measured by a passive cavity aerosol spectrometer probe (PCASP) on the University of North Dakota Citation aircraft to determine the aerosol real refractive index and single-scattering albedo. We also show how the lidar profiles of aerosol extinction and backscattering can be used to apply a relative humidity correction to the PCASP data to more closely represent the size distributions at ambient conditions. Finally, we relate the variations in the measured aerosol optical properties and derived physical characteristics to the meteorological conditions during this experiment.

2. Experimental Data

The lidar data discussed here were acquired during the RCS IOP held at the DOE SGP cloud and radiation testbed (CART) site near Lamont, Oklahoma, in April 1994. *Ferrare et al.* [this issue] give a more complete description of this experiment as well as the procedures used to analyze the GSFC Scanning Raman Lidar (SRL) data. The Citation aircraft from the University of North Dakota flew above the SRL lidar during the RCS IOP on April 21 and 24. This aircraft carried a condensation nuclei (CN) particle counter which measured the total number of particles with diameters between 0.01 and 3.0 μm as well as a Particle Measuring Systems PCASP-100X particle probe which measured the number of particles in 15 size bins between 0.1 and 3.0 μm. *Strapp et al.* [1992] give a brief description of the PCASP-100X. On the night of April 21 the Citation flew a stepped ascent pattern between altitudes of 500 and 5500 m, between 0405 and 0545 UT, and a spiral descent pattern between these same altitudes between 0545 and 0620 UT. The lidar data acquired during the ascent are grouped into 4–5 min averages corresponding to the period the aircraft flew at a constant altitude. During the descent the data were averaged every 2 min.

During these aircraft observations the SRL acquired data at three scan angles: 0°, 80°, and 85° measured from the zenith. Because vertical profiles were acquired twice as often as the other angles, six consecutive vertical profiles were averaged together, while three consecutive profiles at each angle were averaged to reduce the random error in the data. Thus the data from each angle has an effective temporal resolution of 12 min. The resulting profiles at the three scan angles are combined to form profiles extending as close to the surface as possible; for water vapor, relative humidity, and aerosol backscattering, the minimum altitude was 15 m, while the minimum altitude for aerosol extinction was 90 m. Plate 1 shows images of water vapor mixing ratio, relative humidity, aerosol backscattering, and aerosol extinction constructed using these SRL profiles. The temperature and density profiles measured by three radiosondes, launched at 0100, 0400, and 0700 UT, are used along with the SRL data to derive relative humidity and aerosol backscattering.

Several features should be noted in these images. First, while the highest concentration of water vapor is near the ground and increases throughout the night, the highest relative humidities occur between 1 and 2 km. Second, both the water vapor and the aerosol images show that there is an elevated layer of water vapor and aerosols with highest concentrations of water vapor and aerosols just above 4 km. Third, there is an increase in both aerosol backscattering and extinction throughout the lowest 1.5 km beginning between 4 and 5 UT. There is a more pronounced aerosol feature within the lowest 400 m which begins to appear around 0700 UT.

A comparison between the lidar and aircraft PCASP aerosol profiles on April 21 is shown in Figure 1. Profiles of the aerosol backscattering coefficient, extinction coefficient, and extinction/backscattering ratio derived from the lidar data are shown along with the total number of particles in the size range 0.1–3.0 μm derived from the PCASP measurements. The lidar profiles shown in this figure are constructed by matching the appropriate lidar profile to the time and altitude of the aircraft measurement. Since the uncertainty in the aerosol extinction coefficient is greater than 100% for altitudes between 2 and 3.5 km, the aerosol extinction/backscattering coefficient is not shown for this region. Figure 1 shows that the largest values of aerosol backscattering and extinction measured by the lidar and the highest number of aerosol particles measured on the aircraft were observed for altitudes below 2 km.

The increase in the number of particles measured by the PCASP between aircraft ascent and descent is consistent with the increase in the aerosol backscattering and extinction measured by the lidar. Note also that the aerosol extinction/backscattering ratio S_a, measured by the lidar within the lowest 2 km, also increased slightly with time and that the aerosol extinction/backscatter ratio decreased from about 60–70 sr in the lower layer to between 40 and 50 sr in the elevated layer near 4 km. In section 3, we will show how these changes in S_a are indicative of changes in the physical characteristics (i.e., size, shape, and/or composition) of these aerosols.

This change in aerosol physical characteristics as a function of altitude is also supported by a change in the aerosol size distribution measured by the PCASP. Figure 2 shows representative size distributions for aerosols in the lower altitudes of 0.63 km (ascent) and 0.7 km (descent), while distributions for the upper layers are represented at altitudes at 4.6 km (ascent) and 4.5 km (descent). The values at the radius of 0.025 μm were estimated by subtracting the total amount of particles measured by the PCASP (0.1–3.0 μm) from the total measured by the CN counter (0.01–3.0 μm). The PCASP was calibrated during the IOP using polystyrene latex beads, and the measured size distributions were within the manufacturer's specifications. A constant volume pump controls flow through the probe; flow rates were also checked during calibrations and found to be within normal range. No corrections are made to account for changes in the size distributions caused by drying of the samples before

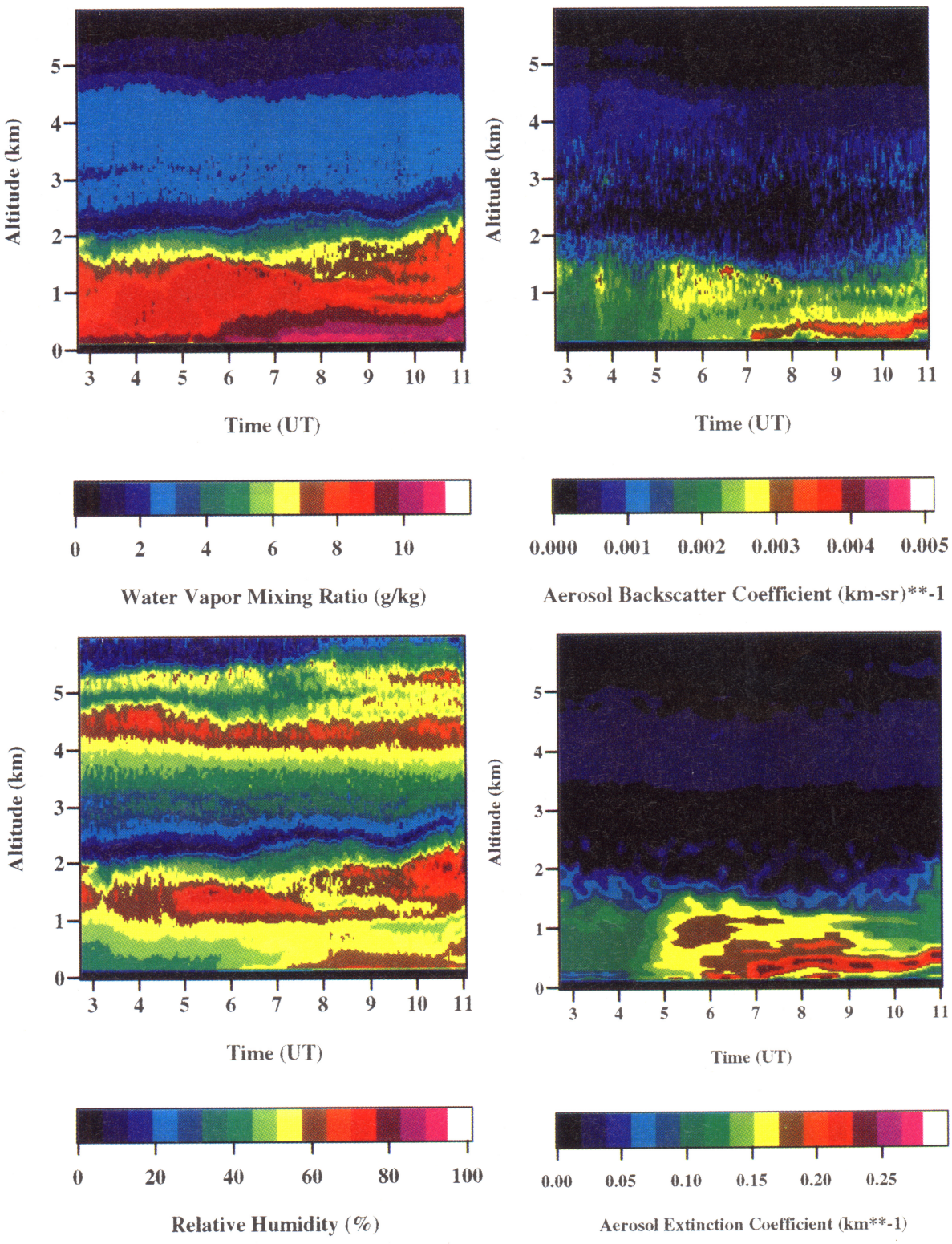

Plate 1. Water vapor mixing ratio (top left), relative humidity (bottom left), aerosol backscattering coefficient (top right), and aerosol extinction coefficient (bottom right) measured by the Scanning Raman Lidar (SRL) on April 21, 1994, during the remote cloud sensing intensive operations period (RCS IOP).

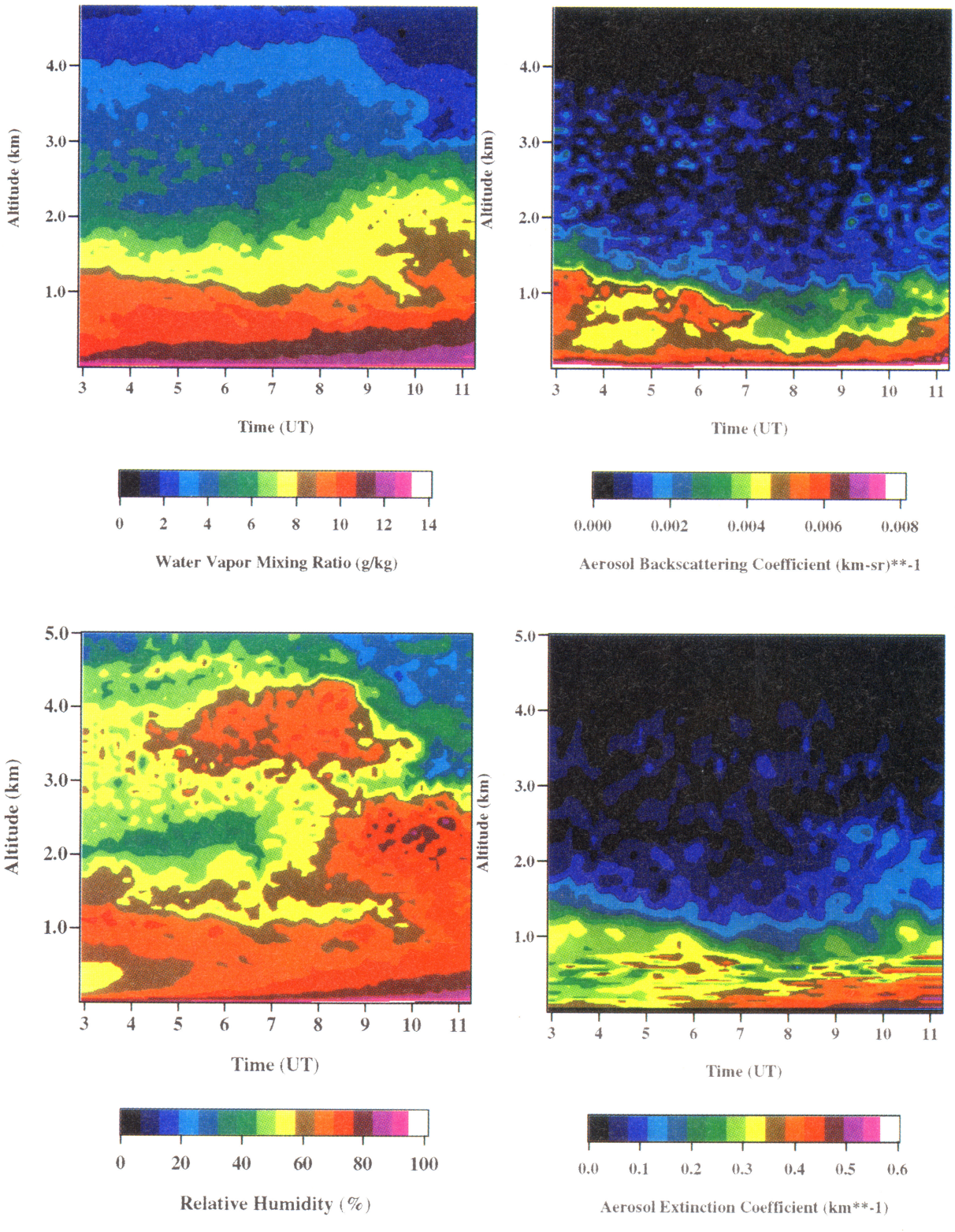

Plate 2. Water vapor mixing ratio (top left), relative humidity (bottom left), aerosol backscattering coefficient (top right), and aerosol extinction coefficient (bottom right) measured by the SRL on the night of April 24, 1994, during the RCS IOP.

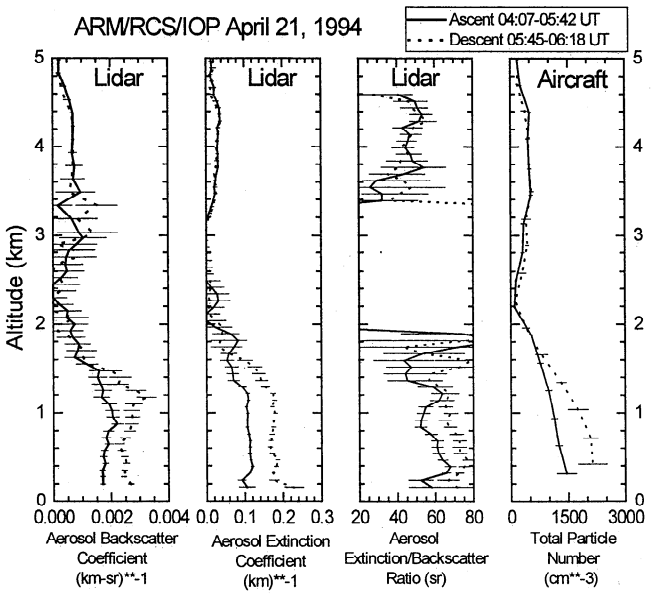

Figure 1. Profiles of aerosol backscattering, extinction, and extinction/backscatter ratio measured by the SRL (left panels) during the ascent and descent on the University of North Dakota (UND) Citation on April 21, 1994, during the RCS IOP. Right panel shows the total number of particles measured by the passive cavity aerosol spectrometer probe (PCASP) instrument on the aircraft. The error bars for the lidar profiles correspond to the uncertainty in the data associated with the random error in the lidar measurements; these random errors are computed using Poisson statistics (i.e., the standard deviation is given by the square root of the total number of photon counts). The error bars for the total particle number measured on the aircraft correspond to the standard deviation of the number of particles computed for each of the 4–5 min averages when the aircraft flew at a constant altitude.

measurement [*Strapp et al.*, 1992]. These effects and associated corrections are discussed in section 3. Figure 2 shows that there was an increase in the number of accumulation mode particles with radii near 0.1 μm in the lower layer. In addition, the number of particles in the lower layer increased with time between aircraft ascent and descent.

The aircraft flew a somewhat similar ascent and descent pattern on the night of April 24 with ascent between 0318 and 0357 UT and descent between 0431 and 0509 UT. The water vapor mixing ratio, relative humidity, aerosol backscattering, and aerosol extinction images derived from the lidar data on this night are shown in Plate 2. These profiles and images are constructed in the same manner as for April 21. The lidar imagery show that the aerosols are concentrated in the lowest kilometer during the night with a small increase in the backscattering and extinction coefficients with time in the lowest few hundred meters. The elevated layer of aerosols observed on the night of April 21 is not observed on April 24. The aerosol size distributions measured by the PCASP instrument are shown in Figure 3; this figure shows the decrease in the accumulation mode particles between altitudes of 1 km and 4 km and that the shape of the size distributions remained nearly constant between aircraft ascent and descent. The accumulation mode aerosol volume increased slightly with time. The lidar profiles also show an increase in the aerosol scattering and extinction coefficients with time and a slight increase in the aerosol extinction/backscattering ratio. In the next section, we use Mie theory to examine in more detail the comparison of the aerosol optical parameters measured by the lidar with the size distributions measured by the aircraft PCASP instrument.

3. Retrieval of Aerosol Physical Properties

By comparing the lidar measurements of aerosol extinction and extinction/backscattering, water vapor mixing ratio and relative humidity with the PCASP measurements of the dry aerosol size distribution, we shall now discuss how the ambient aerosol size distribution is estimated as well as the aerosol real refractive index and single-scattering albedo.

3.1. Mie Computations

Although the measurements described in section 2 show that the vertical and temporal variations in the aerosol backscattering and extinction profiles derived from the lidar data are consistent with the size distributions measured by the PCASP instrument, it is difficult to directly compare the two measurements. However, the aerosol extinction and backscattering coefficients corresponding to the aerosol size distributions measured by the PCASP instrument can be computed using Mie theory and compared to the lidar measurements. *Brock et al.* [1990] report on a similar comparison using airborne lidar measurements of aerosol backscattering and ASASP-X measurements of aerosol size distributions to study Arctic haze. In that study they used lidar measurements of aerosol backscattering along with nephelometer measurements of aerosol scattering to estimate the ratio of scattering to backscattering. *Takamura and Sasano* [1990] used simultaneous lidar and Sun photometer measurements along with measurements of particle size to estimate the aerosol refractive index. However, the value of S_a used to invert the lidar measurements of aerosol backscattering to extinction had to be determined from the Sun photometer measurements of aerosol optical thickness and the measured aerosol size distributions. *Rosen et al.* [1992] compared backscattering measured by a ground-based lidar and by a backscattersonde with that computed from coincident particle size distribution measurements and found that aerosol optical properties can be estimated using size distributions inferred from optical particle counters.

When using Mie theory to compute aerosol optical properties using aerosol physical characteristics, the aerosols are usually assumed to be spherical. Using Mie theory to compute aerosol optical properties when large amounts of nonspherical aerosols are present can lead to incorrect results [*Koepke and Hess*, 1988; *von Hoyningen-Huene and Wendisch*, 1994; *Mishchenko et al.*, 1995]; however, for aerosols that have a small number of large aerosols, such as for continental or urban aerosols, the scattering functions can be sufficiently calculated with Mie theory [*Koepke and Hess*, 1988]. In addition, those water-soluble small particles in the accumulation mode become more spherical as they acquire water with increasing relative humidity [*Hanel*, 1976; *Nilsson*, 1979].

The effects that various particle sizes have on aerosol optical properties varies with wavelength. Since the deviation from Mie scattering caused by nonspherical particles increases with increasing particle size [*Koepke and Hess*, 1988], the effects nonspherical particles have on the optical properties will also vary with wavelength. Therefore as an additional test, we computed the contributions made by various sizes of aerosols on aerosol scattering and extinction as a function of wavelength. For this example, the aerosol size distribution is derived from solar almucantar measurements acquired by the CIMEL Sun photometer on April 20 following the methods described by

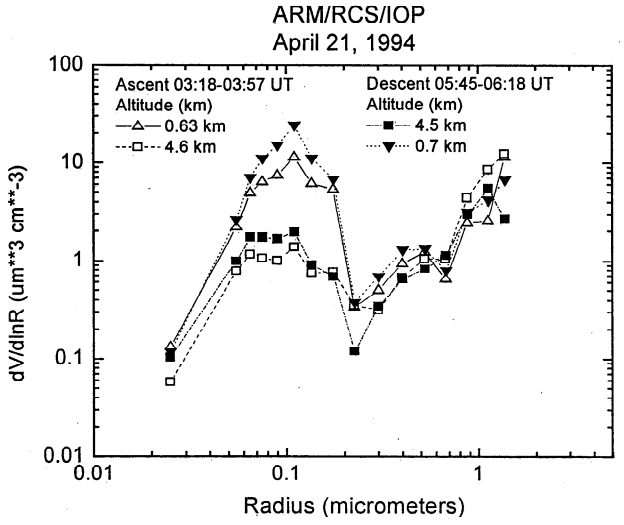

Figure 2. Aerosol volume size distributions measured by the PCASP instrument flown on the UND Citation on April 21, 1994, during the RCS IOP.

Kaufman et al. [1994] and *Remer et al.* [1997]. Using this size distribution, the resulting contribution to the aerosol extinction coefficient is computed as a function of particle size for three wavelengths, 351 nm (SRL), 530 nm, and 1069 nm, which represent typical laser wavelengths in the UV, visible, and near-IR parts of the spectrum. These contributions, along with the size distribution used for this test, are shown in Figure 4. For 351 nm, aerosol extinction and backscattering are most sensitive to particle radii between about 0.06 and 0.7 μm; the size range increases to 0.08 to 1.5 μm for 530 nm and 0.1 to 3.0 μm for 1069 nm. Thus for the typical size ranges observed during the RCS IOP, aerosol optical properties at 351 nm are much less sensitive to coarse mode particles (radii > 1.0 μm) than the optical properties in the visible and near infrared, so nonspherical particles should not significantly impact the Mie computations at 351 nm. This also indicates that aerosol optical properties at 351 nm are also less sensitive to the different composition ($CaCO_3$, SiO_2, etc.) of coarse mode particles.

3.2. Relative Humidity Correction

The measurements of particle size acquired by the PCASP instrument permit the computation of aerosol extinction and backscattering. However, these size distribution measurements do not necessarily represent those at ambient conditions. *Strapp et al.* [1992] point out that the deiced PCASP probe dries the aerosols before measurement. These results were found by comparing the PCASP aerosol size measurements with those measured by a FSSP-300 (forward scattering spectrometer probe) instrument that did not dry the aerosols and therefore measured the hydrated aerosols. Consequently, they found that only by applying corrections to account for hygroscopic aerosol growth with increasing relative humidity did the size distributions measured by the PCASP agree with those simultaneously measured by a FSSP-300 instrument.

In the present study, it is not possible to unambiguously determine the ambient aerosol size distribution from the PCASP measurements alone. However, by comparing the aerosol extinction and backscattering derived from the PCASP measurements with the values derived from the lidar measurements at appropriate altitudes, an appropriate humidity correction can be applied to the PCASP data. When this correction is determined, the optical properties derived from the lidar data and from the PCASP data can be examined to learn how the aerosol optical properties are related to the aerosol physical characteristics.

Because many atmospheric aerosols are hygroscopic and therefore absorb water, their physical size and composition change as a function of relative humidity. This change in the particle size with relative humidity has been studied in detail for several types of atmospheric aerosols in the laboratory [*Tang*, 1976; *Tang et al.*, 1978; *Sloane and Wolff*, 1985; *Sloane*, 1986] and in measurements in the atmosphere near the surface [*Charlson et al.*, 1984; *Hanel*, 1976; *Svenningson et al.*, 1992]. However, because atmospheric aerosols are invariably mixtures of various substances which behave differently with changes in relative humidity and because the change in particle size also often depends on whether relative humidity is increasing or decreasing, it is difficult to determine an appropriate single aerosol substance to characterize the relationship between particle size and relative humidity in the atmosphere. Therefore we have used a simpler relationship to parameterize the change in particle radius with humidity. This humidity correction, which is discussed by *Hanel* [1976] and *Remer et al.* [1997], states that the change in particle radius with relative humidity is given by

$$\frac{r(\mathrm{RH}_1)}{r(\mathrm{RH}_2)} = \left(\frac{1 - \frac{\mathrm{RH}_1}{100}}{1 - \frac{\mathrm{RH}_2}{100}} \right)^{-\gamma} \tag{1}$$

The exponent γ has values that typically range from 0.1 to 0.3 [*McMurry and Stolzenburg*, 1989; *Svenningson et al.*, 1992]. In this expression the value of $\mathrm{RH}_2 = 40$ (relative humidity = 40%) is used as a reference. Both the FSSP-300 and the PCASP-100X probes appear to measure dry aerosol at this relative humidity; in addition, the aerosols appear to be dried by the PCASP heating at all relative humidities up to at least 80% [*Strapp et al.*, 1992]. These growth factors are valid as long as the particle remains a solution droplet. Using equation (1) and the appropriate PCASP size distributions, we show in section 4 that a value of $\gamma = 0.3 \pm 0.05$ matches the lidar profiles of extinction and extinction/backscattering.

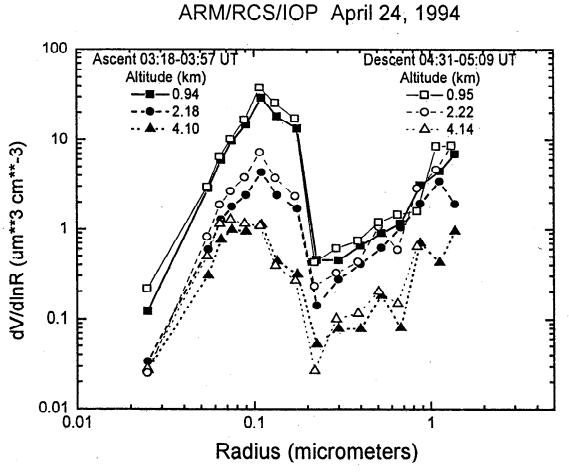

Figure 3. Aerosol volume size distributions measured by the PCASP instrument flown on the UND Citation on April 24, 1994, during the RCS IOP.

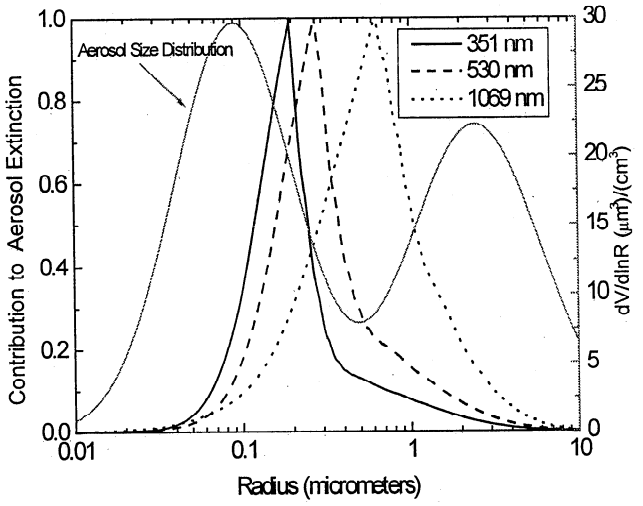

Figure 4. Contribution to aerosol extinction for various aerosol sizes (left axis). Aerosol extinction is computed using the aerosol size distribution (right axis) derived from solar almucantar measurements acquired by the CIMEL Sun photometer on April 20, 1994, following the methods described by *Kaufman et al.* [1994] and *Remer et al.* [1997]. Aerosol extinction is computed using Mie theory by varying both the beginning and the ending radii from their starting values of 0.001 μm and 20 μm. Normalized extinction is computed by dividing by the aerosol extinction derived using the entire size range of particles.

The Mie calculations of aerosol extinction and backscattering require both the size and distribution and the refractive index of particles. The complex refractive index, which depends on the composition of the particles, is also unknown. For the models that follow, the assumption is made that most of the aerosols consist of weakly absorbing particles with an imaginary index $k < 10^{-4}$ mixed with a small number of highly absorbing aerosols with k~1.0 [*Fraser et al.*, 1992]. Other aerosol models [*Shettle and Fenn*, 1979; *d'Almeida et al.*, 1991] chose to represent such mixtures with a composite imaginary refractive index with $0.001 < k < 0.1$ which is close to the values obtained by various remote sensing and in situ techniques [*Patterson and Grams*, 1984; *Reagan et al.*, 1980; *Takamura et al.*, 1994]. However, this is not used here because *Bohren and Hoffman* [1983] point out that no common atmospheric aerosol substance exists which has an imaginary refractive index in this range. Therefore for the computations that follow, the imaginary index for a weakly absorbing aerosol such as ammonium sulfate is used. The absorbing particles are assumed to be much smaller than the wavelength and that they exist as distinct particles (external mixture). The scattering effects of these absorbing aerosols are small relative to their absorbing effects [*Fraser and Kaufman*, 1985]. In this method, aerosol absorption is parameterized by the single-scattering albedo ω_0, rather than by the imaginary refractive index. The implications of this parameterization on the derived single-scattering albedo will be discussed in section 3.3.

The calculations which follow rely on determining three parameters, the relative humidity correction γ, the real refractive index n, and the single-scattering albedo, ω_0, such that the aerosol extinction and backscattering profiles computed from the aerosol size distribution measured on the aircraft match the corresponding profiles measured by the lidar. In solving for the real refractive index the effect of changes in relative humidity on the refractive index is also included since the composition of the aerosols change as water is either added or removed during changes in relative humidity. The variation in the real refractive index with relative humidity is modeled using the relation given by *Hanel* [1984] which states that the real refractive index is given by

$$n(\mathrm{RH}) = n_w + (n_0 - n_w)\left[\frac{r(\mathrm{RH}, r_0)}{r_0}\right]^{-3} \quad (2)$$

where n_0 is the dry value, n_w is the real refractive index of water, r_0 is dry particle radius, and r (RH, r_0) is the particle radius at the ambient relative humidity RH.

3.3. Application

Before discussing the procedures used to determine the real refractive index, single-scattering albedo, and the humidity correction factors, we shall first examine the sensitivities of aerosol extinction and the extinction/backscattering ratio to γ, n, and ω_0 at 351 nm. For these tests we have used a single lognormal size distribution corresponding to the accumulation mode of the AFGL (Air Force Geophysical Laboratory) [*Shettle and Fenn*, 1979] rural model with a mean modal radius of $r_i = 0.0285$ μm, standard deviation of the natural logarithm of the radius of $\sigma_i = 0.693$, refractive index of $n = 1.43$, and a single-scattering albedo of 0.95 [*Kaufman and Fraser*, 1983]. The results that follow are for this single "typical" size distribution and so may not be representative for the wide variety of aerosol size distributions observed in the atmosphere. Figure 5 shows the variation in the aerosol extinction as a function of relative humidity and the exponent γ from equation (1). The aerosol extinction was normalized to unity at RH = 40%. This figure shows that aerosol extinction is sensitive to the value of γ, varying by a factor of nearly 2 at RH = 80% as γ varies between 0.1 and 0.3. In contrast, Figure 5 (right) shows that the extinction/backscattering ratio increases only slightly between 65 and 75 sr for this same increase in γ. This result is consistent with that reported by *de Leeuw et al.* [1986] and *Takamura and Sasano* [1987] who also found that the dependence of S_a on relative humidity was small. Figure 6 shows how the increases in aerosol

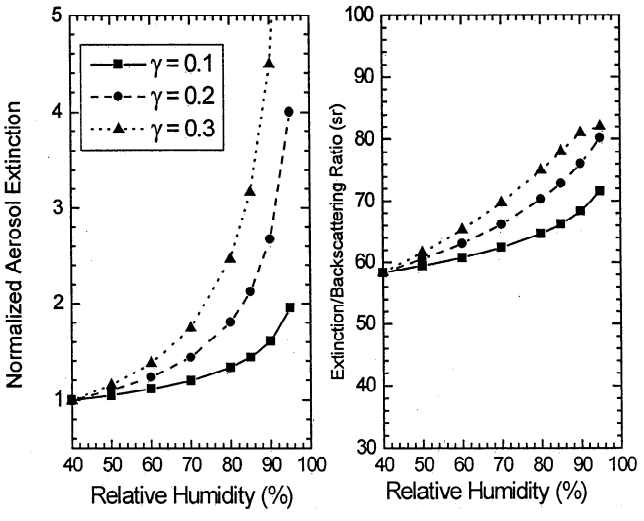

Figure 5. (left) Variation in aerosol extinction with relative humidity as a function of the parameter γ from equation (1). Aerosol extinction is normalized to unity at RH = 40%. (right) Same for the aerosol extinction/backscatter ratio S_a.

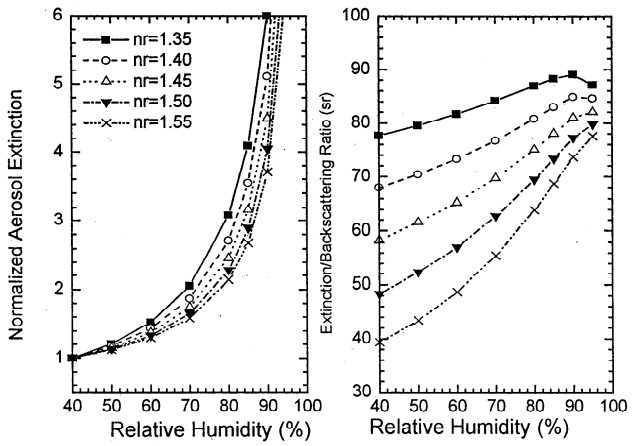

Figure 6. (left) The variation in aerosol extinction with relative humidity as a function of the real refractive index. Aerosol extinction is normalized to unity at RH = 40%. (right) Same for the aerosol extinction/backscatter ratio S_a.

extinction and S_a with relative humidity vary with changes in the real part of the refractive index. For these cases the exponent $\gamma = 0.3$ is used. These figures show that both the extinction and the extinction/backscattering ratio vary with changes in the real part of the refractive index. Figure 7 shows how the relationships of aerosol extinction S_a with relative humidity depend on ω_0. In this case of constant refractive index, aerosol extinction is relatively insensitive to ω_0, while the extinction/backscattering ratio varies with ω_0. The variation in the aerosol extinction and extinction/backscattering with altitude as revealed by the lidar data provides additional information used to determine these parameters.

Examples of how variations in the relative humidity exponent γ, real refractive index n, and single-scattering albedo ω_0 affect the aerosol extinction and extinction/backscattering ratio derived from the measured size distribution are shown in Figure 8. Here the PCASP aerosol size distribution is used to compute aerosol extinction and the extinction/backscattering ratio for each altitude between 600 and 4700 m during the descent of the aircraft between 0545 and 0618 UT on April 21 during the RCS IOP. The aerosol extinction and extinction/backscattering profiles derived from the lidar data are also shown; these profiles have been constructed using the appropriate times of the lidar data to match the altitude of the aircraft. Figures 8a and 8b show the effect of various values of the relative humidity correction factor γ on aerosol extinction and extinction/backscattering, respectively. Also shown are the profiles derived using no humidity correction. The aerosol extinction/backscattering ratio derived from the lidar data is not shown for altitudes between 1.7 and 3.5 km since the low values of aerosol extinction are within the random error in the lidar data. The correction for particle growth due to variations in relative humidity is largest in the lowest 1.5 km where the relative humidity measured by the EG&G dew point hygrometer on the aircraft increased from 60 to 80% between altitudes of 0.7 and 1.4 km. The real refractive index of the dry particles used to compute the profiles shown in Figures 8a and 8b is $n_0 = 1.47$; these values are also corrected for changes in relative humidity using equation (2). Since the relative humidity varies between 60 and 80% in the layer below 1.5 km, the effect of the relative humidity correction parameter γ on the shape of aerosol extinction profile in this region is pronounced and is therefore used to determine the appropriate value of the correction parameter of $\gamma = 0.3$.

The effects on aerosol extinction and the extinction/backscattering ratio produced by varying the real refractive index are shown in Figures 8c and 8d. These figures show that increasing the refractive index from 1.4 to 1.5 increases the aerosol extinction while conversely, decreasing S_a. This indicates that aerosol backscattering increases more rapidly with refractive index than extinction. In addition, these figures show that varying

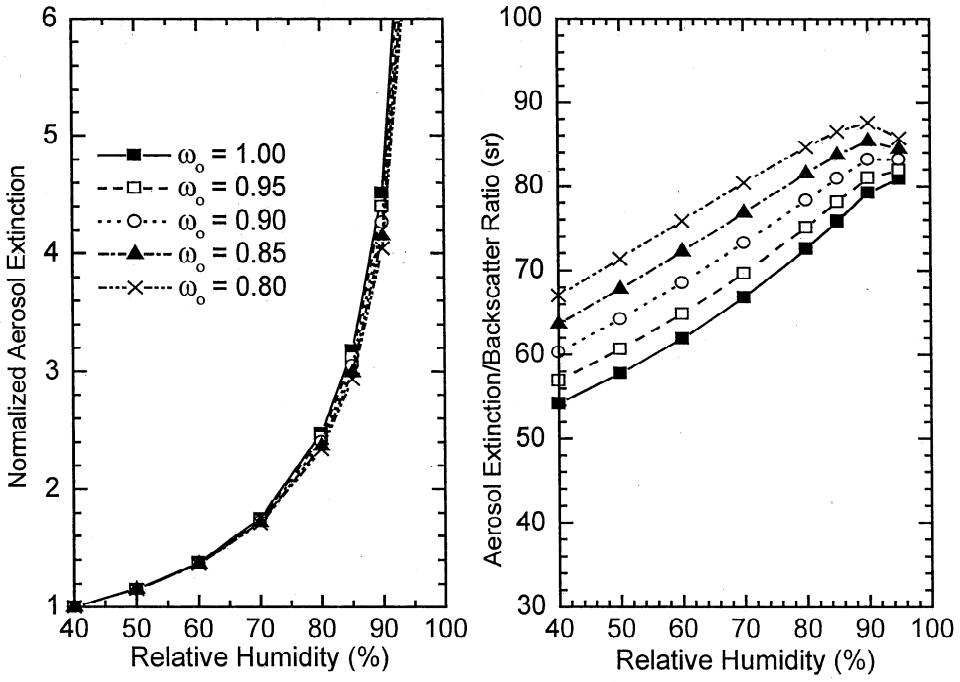

Figure 7. (left) Variation in aerosol extinction with relative humidity as a function of the single-scattering albedo. Aerosol extinction is normalized to unity at RH = 40%. (right) Same for the aerosol extinction/backscatter ratio S_a.

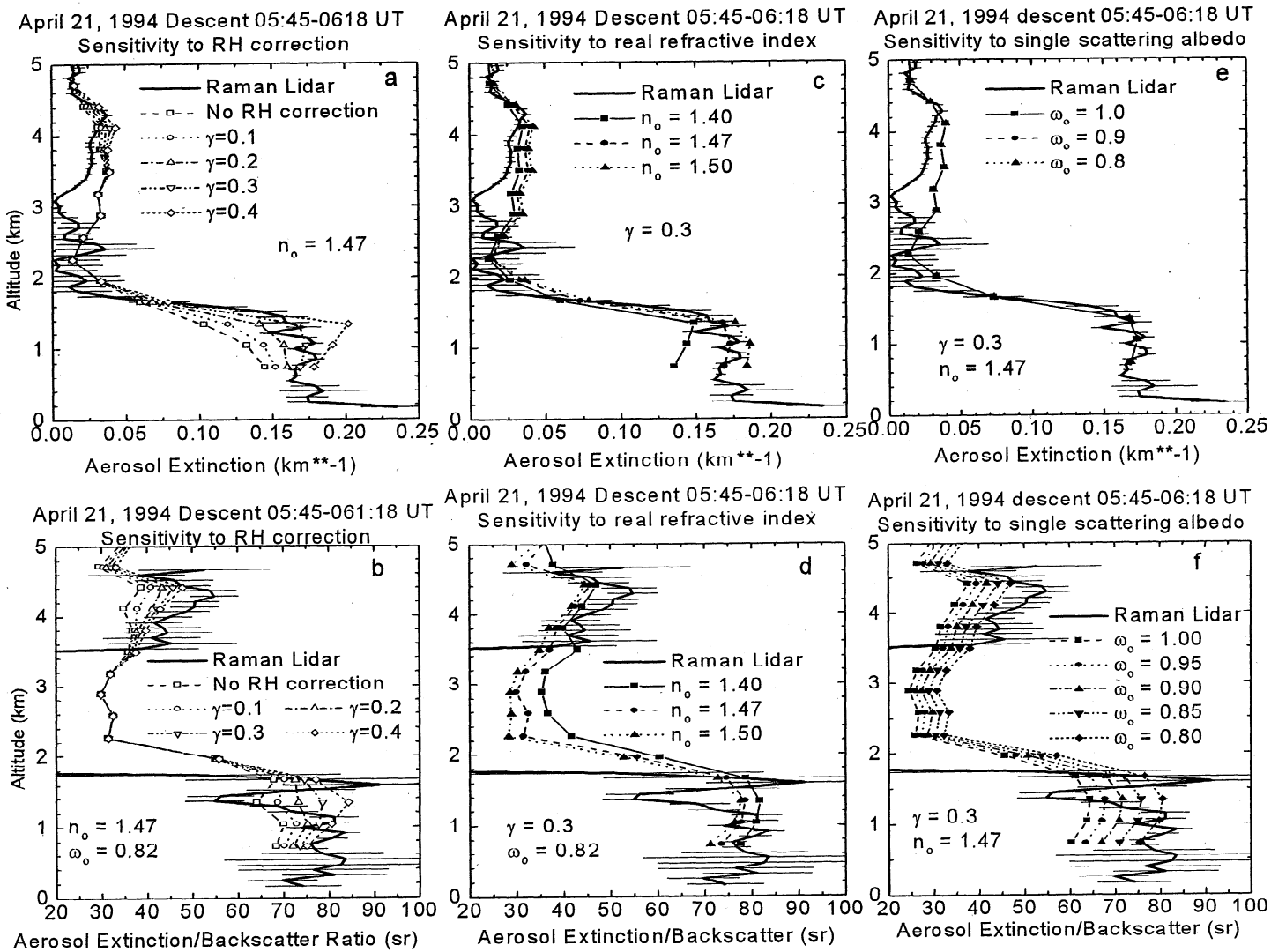

Figure 8. (a, c, e) Profiles of aerosol extinction and (b, d, f) aerosol extinction/backscattering ratio derived from SRL data and UND Citation aircraft PCASP size distributions on April 21, 1994. The sensitivity of the profiles derived from the size distributions to changes in the particle size relative humidity correction (left), real refractive index (middle), and single-scattering albedo (right). The default parameters used are $n_0 = 1.47$, $\gamma = 0.3$, $\omega_0 = 0.82$. These figures show that the magnitude of the aerosol extinction is sensitive to n_0, the shape of the aerosol extinction profile is sensitive to γ, while the aerosol extinction/backscatter ratio is sensitive to ω_0.

the real refractive index of the dry particles has its greatest impact on the magnitude of aerosol extinction; the change in aerosol extinction with altitude is also slightly altered. Therefore assuming that the real refractive index of the dry particles does not vary significantly in this altitude region, the variation of aerosol extinction with altitude can be used to determine the appropriate relative humidity correction parameter. Figure 8d also shows that the real refractive index varies between the lower layer (below 1.6 km) and the upper layer (between 3.5 and 4.7 km) since a value of $n = 1.47$ matches the lidar measurements of S_a in the lower layer, while a value of $n = 1.40$ provides a better match to the lidar values in the upper layer.

Figures 8e and 8f show the effects of variations in the single-scattering albedo. As discussed earlier, variations in the single-scattering albedo had little effect on the aerosol extinction but affected the aerosol backscattering coefficient and therefore the extinction/backscattering ratio. When the relative humidity correction factor and real refractive index are determined, the single-scattering albedo is determined from the aerosol extinction/backscattering ratio measured by the lidar. The value of ω_0 chosen using this method depends on how the absorbing particles are assumed to be mixed with the other aerosol particles. *Ackerman and Toon* [1981] calculated the single-scattering albedos that result from several different methods of modeling graphitelike carbon (soot) in these samples. They found that ω_0 varies significantly depending on whether the absorbing particles are modeled as external or internal mixtures. Furthermore, they showed that the scattering phase function in the backward direction depends on the manner in which soot is mixed. The dependence of the backscattering phase function, $P(\gamma, 180°)$, on the manner in which the absorbing material is mixed affects the value of ω_0 derived from the lidar aerosol extinction/backscatter ratio. *Ackerman and Toon* [1981] showed that the phase function of 180° ($P(\gamma, 180°)$) for an external mixture is approximately the same as that for an internal mixture which has a soot core and a sulfate shell but can be significantly larger than when the soot is assumed to be uniformly mixed throughout the particle. Therefore for a given value of S_a an external mixture can be expected to produce a smaller value of ω_0 for a given amount of soot than a mixture where the soot is mixed uniformly throughout the particle. Using the assumed external mixture, a value of $\omega_0 = 0.8$ is required to match the lidar profiles of S_a in the lower layer. However, if aerosol absorption is instead modeled by using an "effective" (nonphysical) value of the imaginary index of refraction of $k = 0.009$, then a value of $\omega_0 = 0.94$ is obtained. In addition, *Ackerman and Toon* [1981] also state that the role that external and internal mixtures have on ω_0 depends also whether the soot is added to accumluation mode particle ($r < 1$ μm) or added to coarse mode particles ($r > 1$ μm). *Heintzenberg et al.* [1997] point out that the retrievals of single-scattering albedo using inverse methods, as discussed here, lead to nonunique solutions; the derived values of ω_0 do represent a measure of the optical properties of the atmosphere but only for the case in which these assumptions are valid.

3.4. Procedure

By matching profiles of aerosol extinction and extinction/backscattering computed from the aerosol size distributions measured by the PCASP instrument on the nights of April 21 and 24 to the coincident lidar profiles of aerosol extinction and extinction/backscattering ratio, estimates of the relative humidity correction factor, real refractive index, and single-scattering albedo are determined. This process proceeds in an iterative manner. First, the relative humidity correction factor γ is derived from those times when the lidar measurements showed that the aerosol extinction and relative humidity varied with altitude and the extinction/backscattering ratio is nearly constant with altitude. Since S_a is relatively insensitive to γ but varies with the real part of the refractive index, those times and altitudes where the aerosol extinction varies with altitude, but S_a remains relatively constant, are indicative of changes in aerosol size with relative humidity; these regions can be used to estimate the humidity correction factor γ and the real refractive index. Next, using equation (2) and this relative humidity profile, the profiles of dry and wet real refractive indices used to compute the aerosol extinction profile which most closely matches the lidar aerosol extinction profile are determined. This process proceeds until the mean rms error between the computed aerosol extinction profile and the measured profile is less than 0.01 km^{-1}. Finally, using the derived values of a humidity correction factor and the real refractive index, the single-scattering albedo is chosen by minimizing the mean rms difference between the measured and the computed profiles of the extinction/backscattering ratio S_a.

4. Results

Figure 9 summarizes these results for measurements acquired during the descent of the aircraft between 0545 and 0618 UT on April 21. This is the same period as shown in Figure 8. The variation in relative humidity with altitude is shown in Figure 9a. A value of the relative humidity correction factor $\gamma = 0.3 \pm 0.05$ is derived for these measurements. The profiles of dry and wet real refractive indices used to derive the aerosol extinction profile are shown in Figure 9b, while the single-scattering albedo profile is shown in Figure 9c. The resulting profiles of aerosol extinction, backscattering, and extinction/backscattering ratio derived from the PCASP data in this manner are shown in Figures 9d, 9e, 9f along with the corresponding lidar profiles. Figure 10 shows similar results for measurements acquired during aircraft ascent between 0407 and 0542 UT. In both the ascent and the descent cases the profiles derived from the aircraft PCASP size distribution measurements match the lidar profiles very well; this is especially true for the measurements acquired below 1.5 km. In both cases the aerosol extinction and backscattering profiles derived from PCASP measurements for altitudes between 3.0 and 4.5 km are slightly larger than those measured by the SRL; this difference remained regardless of the refractive indices chosen. The reason for this difference is not clear at this time but may be due to uncertainties in the coarse mode particle size distribution measured by PCASP instrument as well as aerosol extinction and backscattering sensitivity limits of the SRL. However, the aerosol extinction/backscattering ratios derived from the PCASP measurements matches the SRL values in the upper layer as well as the lower layer. The profiles measured by the SRL and derived from the PCASP measurements both show increases in the aerosol extinction and backscattering in the lower layer between aircraft ascent (0407 and 0542 UT) and descent (0545 and 0618 UT). Note also that the aerosol extinction/backscattering ratio derived from the two different measurements both show an increase from $S_a = 55$–60 during ascent to $S_a = 75$–80 during descent. Recall that Plate 1, which shows the lidar aerosol backscattering and extinction on this night, indicates a clear increase in aerosol extinction (and aerosol backscattering to a lesser extent) below 1.2 km. In addition, both the aerosol backscattering and the extinction images show a more pronounced layer of aerosols

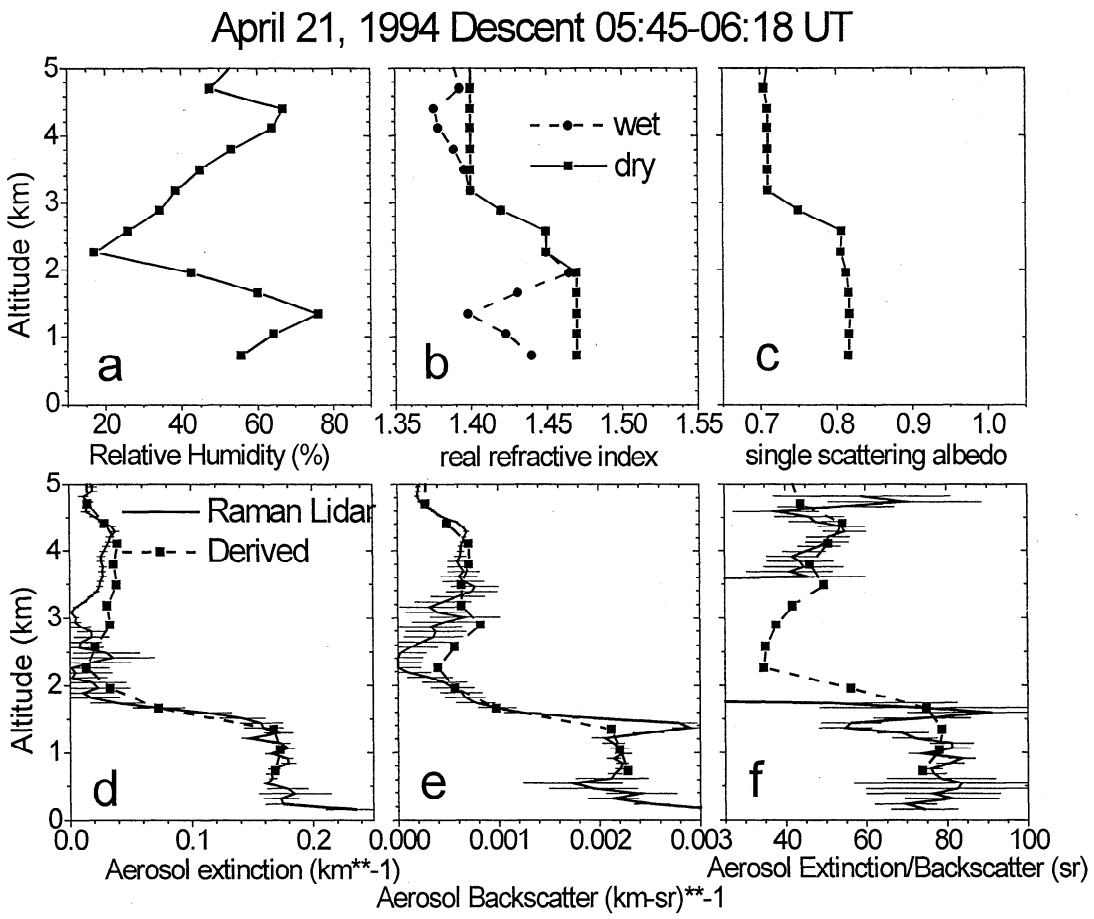

Figure 9. (a) Relative humidity measured by hygrometer during descent of Citation on the night of April 21, 1994. (b) Dry and wet real refractive indices computed for aerosol extinction and backscattering profiles derived using PCASP aerosol size distributions. (c) Derived single-scattering albedos, (d) aerosol extinction coefficient, (e) aerosol backscattering coefficient, and (f) aerosol extinction/backscattering ratio measured by the lidar and derived from the aerosol size distribution measured by the PCASP instrument except for imaginary part of refractive indices.

apparently emanating like a plume from the surface at about 0700 UT after the aircraft measurements. The rapid increase in aerosol extinction and backscattering between 0430 and 0500 UT and the appearance of this plumelike feature around 0700 UT suggests that a different type of aerosol was responsible. Further indications of this are shown in Figures 9b, 9c and 10b, 10c where the real refractive indices and single-scattering albedos corresponding to the aerosol extinction and backscattering profiles derived from the PCASP size distribution measurements are shown. While the real part of the refractive index remained constant at about 1.47 (dry) between ascent and descent, the single-scattering albedo decreased from 0.94 to 0.82. The reason for the decrease in ω_0 and increase in aerosol extinction and extinction/backscattering ratio is not clear; however, the lidar aerosol extinction and backscattering imagery, which shows the appearance of a plumelike feature apparently emanating from near the surface, suggests that the source for these aerosols was close to the site.

Both the real refractive index and the single-scattering albedo remained relatively constant in the upper aerosol layer. The value of $\omega_0 = 0.7$ derived in the upper layer increases to $\omega_0 = 0.92$ if the absorbing material is modeled as an internal volume mixture rather than as an external mixture. The change in size distribution between the lower and the upper aerosol layers also impacts the retrieval of the single-scattering albedo. The size distributions shown in Figure 2 show that the coarse mode becomes more important in this upper layer. *Ackerman and Toon* [1981] found that external mixtures produce lower values of ω_0 compared to internal mixtures when the absorbing particles are added to a size distribution dominated by coarse mode particles. Although the value of $\omega_0 = 0.7$ appears low, it should be noted that *Malm et al.* [1996] found that absorption accounted for about 30% of the aerosol extinction budget for measurements in the western United States.

The aerosol extinction, backscattering, and extinction/backscattering profiles derived from the PCASP size distribution data and the lidar measurements on the night of April 24 are shown in Figures 11 for ascent and 12 for descent. A value of $\gamma = 0.3 \pm 0.05$ is derived for both ascent and descent. These figures also show the values of real refractive index and single-scattering albedos used to derive these profiles. As in the case of April 21, the profiles of aerosol extinction, backscattering, and extinction/backscattering ratio derived from the PCASP measurements agree well with those measured by the lidar. Both methods show the rapid decrease in aerosol extinction and backscattering above 1.2 km and the slight decrease in the thickness of this aerosol layer. The elevated layer of aerosols observed on April 21 was not seen on April 24. Note also that the levels of aerosol extinction and backscattering seen on this day in the lowest kilometer were about twice the levels seen on April 21.

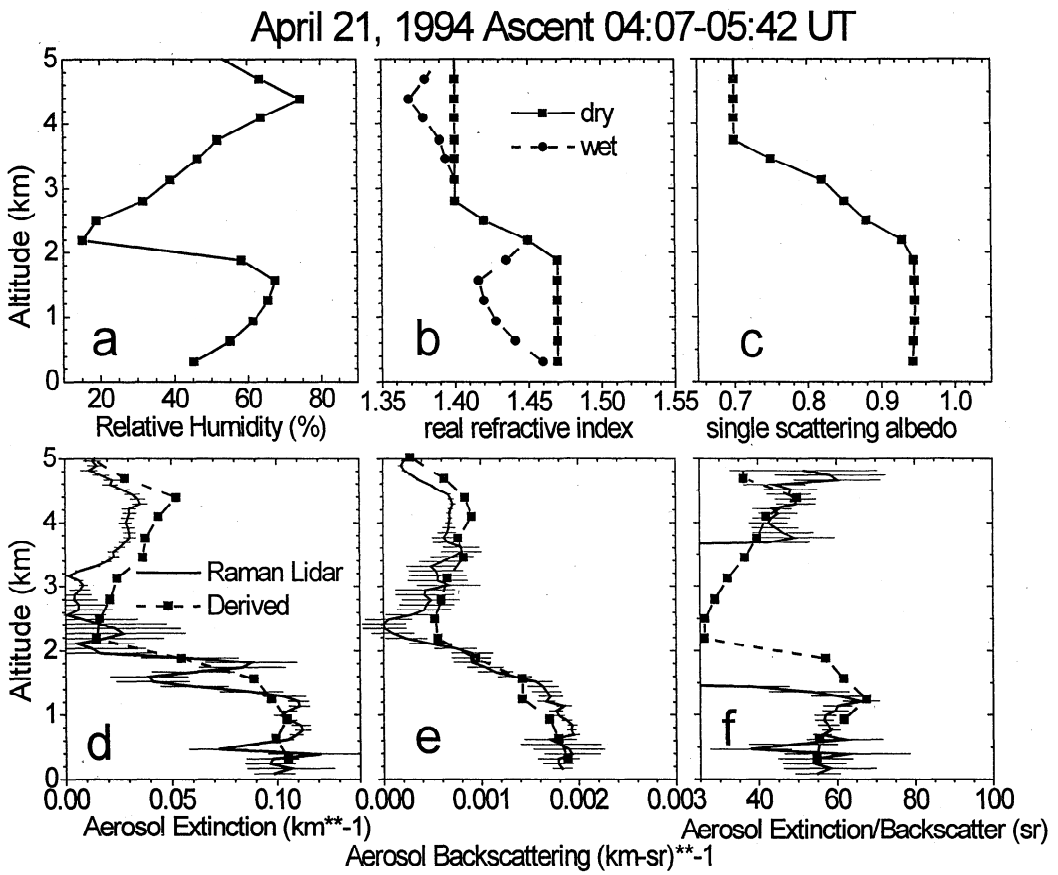

Figure 10. (a) Relative humidity measured by hygrometer during ascent of Citation on the night of April 21, 1994. (b) Dry and wet real refractive indices computed for aerosol extinction and backscattering profiles derived using PCASP aerosol size distributions. (c) Derived single-scattering albedos, (d) aerosol extinction coefficient, (e) aerosol backscattering coefficient, and (f) aerosol extinction/backscattering ratio measured by the lidar and derived from the aerosol size distribution measured by the PCASP instrument except for imaginary part of refractive indices.

The real refractive indices and single-scattering albedos used to derive the aerosol profiles from the PCASP measurements on April 24 are also shown in Figures 11 and 12. The real part, which was 1.50 (dry) during aircraft ascent, decreased to 1.45 (dry) during aircraft descent. The lidar measurements of aerosol extinction and backscattering did not show significant changes between ascent and descent, so the reason for this variation is not known. In both ascent and descent the derived single-scattering albedo was 1.0. Note that during ascent (0318–0357 UT) the derived aerosol extinction/backscattering ratio was larger than that measured by the lidar because the actual derived value of $\omega_0 = 1.1$, required to match the lidar measurements, is not physically possible. The difference indicates that the level of uncertainty in the retrieved single-scattering albedo using this method is approximately 0.1. This error does not account for the uncertainty associated with the assumption of how the absorbing aerosol particles are represented in the aerosol mixture. During descent the derived aerosol extinction/backscattering ratios match those measured by the lidar using a value of $\omega_0 = 1.0$. The aerosol extinction/backscattering ratio values of $S_a = 60$–65 sr observed on this day were slightly higher than those seen during the beginning of the night on April 21 and slightly lower than those seen at the end of this night. Figure 4 in part 1 [*Ferrare et al.*, this issue] showed that the aerosol extinction/backscattering ratio varied during the experiment; these observations, coupled with the change in the refractive indices, suggest that the aerosol composition as well as size distribution varied during this experiment.

Variations in aerosol optical and physical characteristics were also evident in the Sun photometer data. Figure 3 in part 1 [*Ferrare et al.*, this issue], which shows the aerosol optical thickness and precipitable water vapor measured by the SRL at night and by the CIMEL Sun photometer during the day, indicates that the aerosol optical thickness and the precipitable water vapor increased between April 15–16 and April 20–26. In addition, the Sun photometer data indicate that the aerosol size distribution varied during this period. Figure 13 shows the aerosol optical thickness as a function of wavelength for the average of measurements acquired on April 15 (after the cold frontal passage) and on April 24. Previous studies have found that the wavelength dependence of aerosol optical thickness can be represented as $\tau_a \sim \gamma^{-\alpha}$ where α is the Angstrom exponent. The value of α varied between 0.5 on April 15 and 1.5 on April 24. Variations in this exponent are associated with changes in the aerosol size distribution; for example, as α increases from 0.5 to 1.5, the particle size tends to decrease [*van de Hulst*, 1957; *Junge*, 1963].

Aerosol size distributions are derived from the CIMEL Sun photometer almucantar data to show the changes in particle size during this period. This method of retrieving the aerosol size

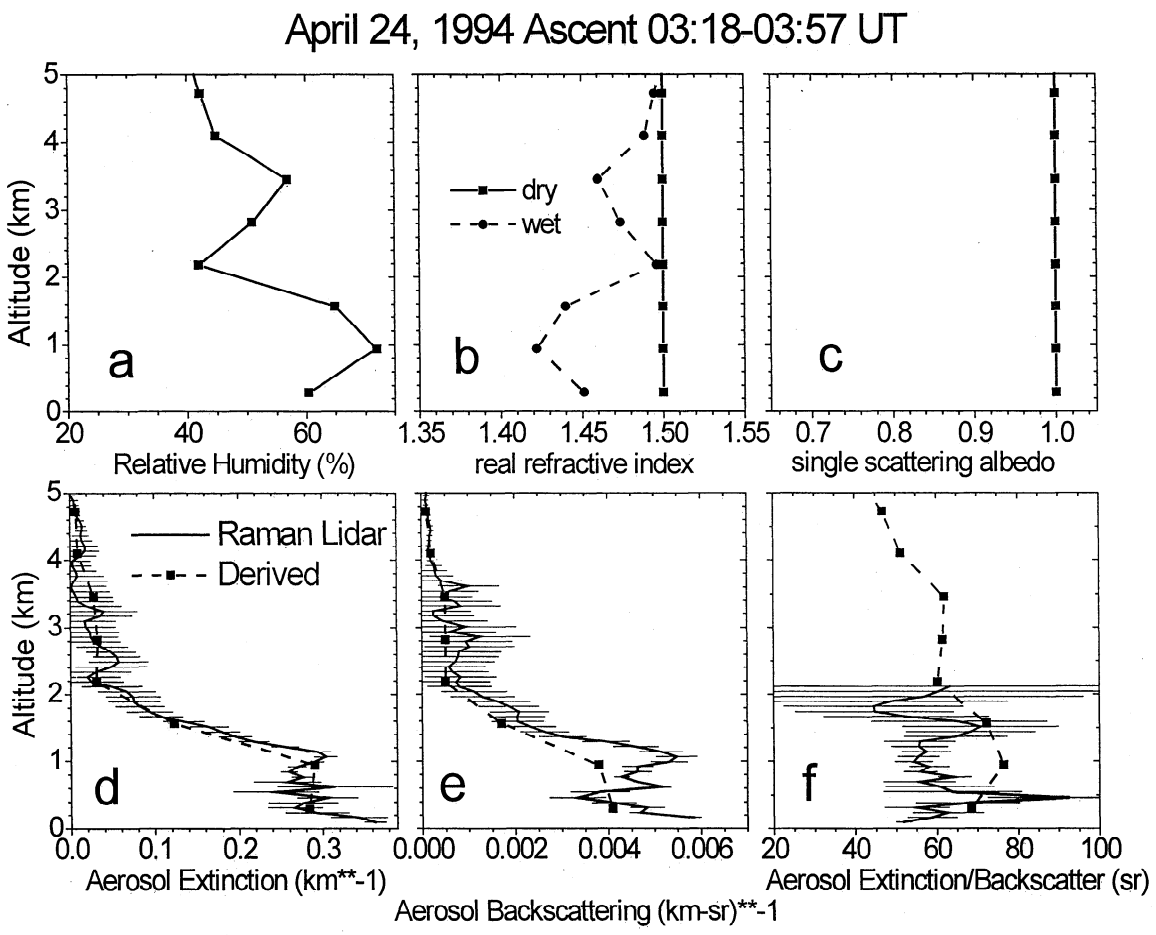

Figure 11. (a) Relative humidity measured by hygrometer during ascent of Citation on the night of April 24, 1994. (b) Dry and wet real refractive indices computed for aerosol extinction and backscattering profiles derived using PCASP acrosol size distributions. (c) Derived single-scattering albedos, (d) acrosol extinction coefficient, (e) aerosol backscattering coefficient, and (f) aerosol extinction/backscattering ratio measured by the lidar and derived from the aerosol size distribution measured by the PCASP instrument except for imaginary part of refractive indices.

distribution, which is based on the algorithm developed by *Nakajima et al.* [1983, 1986] and discussed by *Kaufman et al.* [1994] and *Remer et al.* [1997], uses the Sun and sky radiance measurements acquired by the Sun photometer when the instrument scans in the solar almucantar to derive the aerosol single-scattering phase function and the aerosol size distribution. The aerosol size distributions derived from solar almucantar measurements acquired at the SGP site are shown in Figure 13b. Since the retrieval algorithm produces volume size distributions integrated on the atmospheric column ($\mu m^3/cm^2$), we assume an aerosol scale height of 1.5 km and convert the CIMEL size distribution to true concentration units [*Remer et al.*, 1997]. This scale height is consistent with the mixed layer heights over this period derived from radiosonde and lidar data. The distributions measured on April 15 and 16 are averaged together as were those acquired on April 21 and 24. *Remer et al.* [1997] point out that for aerosol sizes below about 0.15 μm a correction must be applied to account for the overestimate produced by the algorithm. Although this correction was not applied for the distributions shown, it is clear that the amount of accumulation mode aerosols (0.1–1 μm) was about a factor of 3–4 greater on April 21–24 than on April 15–16. The change in these derived size distributions is consistent with the Sun photometer and lidar aerosol optical thickness measurements.

5. Relationship With Meteorological Conditions

The differences in the aerosol sizes and optical properties measured by the lidar, Sun photometer, and aircraft indicate that different types of aerosols were observed during the RCS IOP. Back trajectories were computed to determine if the changes in aerosol properties observed above are correlated with possible source regions of the aerosols. Three day back trajectories were computed using the HYSPLIT3 model [*Draxler*, 1988]. This model uses the meteorological data produced by the National Weather Service nested grid model (NGM) to compute advection and dispersion of air parcels. The model was used to compute three day back trajectories for parcels of air arriving over the SGP site at various altitudes. Figure 14 shows these trajectories for air parcels arriving at the surface at 0600 UT over the SGP on the days listed. The trajectories in Figure 14 show that various air masses were observed by the SRL during the RCS IOP. Between April 15 and April 20, high pressure moved over the site, so winds were light and gradually became more southerly during this period. On April 20 a weak cold front gradually moved over the site and dissipated during the next 24–48 hours. This change in air mass produced the large change in trajectories between April 19 and 20 shown in Figure 14.

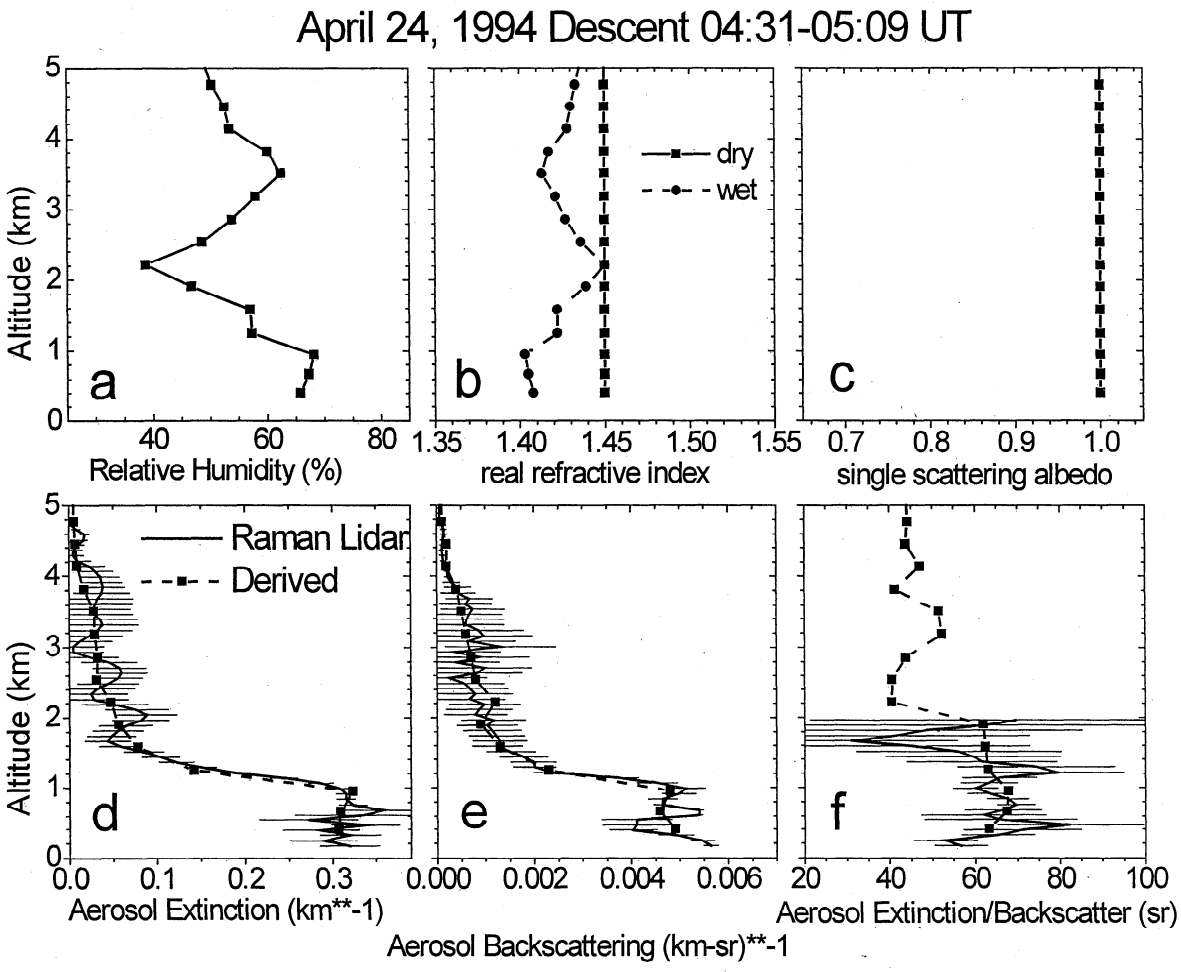

Figure 12. (a) Relative humidity measured by hygrometer during descent of Citation on the night of April 24, 1994. (b) Dry and wet real refractive indices computed for aerosol extinction and backscattering profiles derived using PCASP aerosol size distributions. (c) Derived single-scattering albedos, (d) aerosol extinction coefficient, (e) aerosol backscattering coefficient, and (f) aerosol extinction/backscattering ratio measured by the lidar and derived from the aerosol size distribution measured by the PCASP instrument except for imaginary part of refractive indices.

By April 21 a high pressure system had moved over the SGP, so the air parcels observed over the SGP had traveled from the general vicinity of Oklahoma. There was little variation in either time or altitude for the trajectories observed on this night. Therefore the increases in aerosol scattering and extinction observed by the SRL beginning at 0500 UT shown in Plate 1 and Figure 1 do not appear to be associated with any synoptic scale features. This suggests that the increase in aerosol observed on this night was associated with a local source.

Between April 23 and 25 the trajectories show that air traveling to the SGP had originated generally east to southeast of the site; however, the April 23 trajectories show the air parcels coming from Missouri to the northeast of the site. These trajectories also passed over the more urban areas of St. Louis and the Ohio Valley 48 hours before arriving at the SGP site. Note that the Ohio Valley region in particular has large emissions of sulfur dioxide [*Nizich et al.*, 1995]. The lidar observed the highest values of aerosol extinction and backscattering during the night of April 23; in addition the aerosol extinction/backscattering ratio attained its largest observed values between 70 and 80 sr on this night and on April 24. Higher values of both aerosol extinction and extinction/backscattering ratio are associated with the trajectories that show air parcels had traveled from areas southeast of the site. This is likely due to the higher relative humidities associated with air parcels in close proximity to the Gulf of Mexico. In addition, the Gulf coastal regions southeast of Oklahoma also have large emissions of sulfur dioxide and volatile organic compounds [*Nizich et al.*, 1995].

6. Conclusions

The applicability of a Raman lidar to provide additional information regarding aerosol physical properties is demonstrated using data acquired during the RCS IOP experiment in April 1994. These results represent the first time that simultaneous aerosol extinction and backscattering measurements from a Raman lidar have been used in conjunction with aerosol size distribution measurements to infer the refractive index and single-scattering albedo of tropospheric aerosols. The lidar aerosol backscattering and extinction profiles are used in conjunction with aerosol size distribution measurements acquired by a PCASP particle counter flown on the Citation aircraft from the University of North Dakota to estimate the aerosol hygroscopic growth factor, real refractive index, and single-scattering albedo. Aerosol extinction and backscattering are computed as functions of altitude using the aerosol size distribution measurements and are

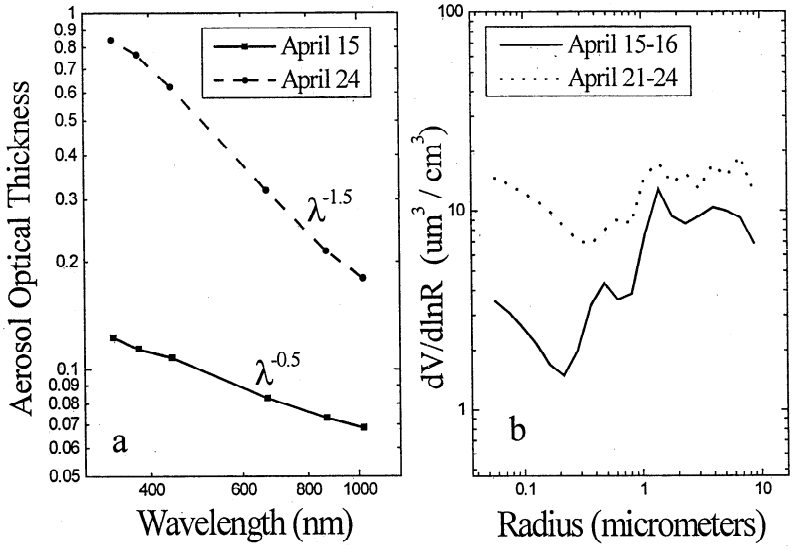

Figure 13. (a) Aerosol optical thickness versus wavelength measured by the CIMEL Sun photometer during the April 1994 RCS IOP. (b) Aerosol volume size distributions derived from the solar almucantar measurements acquired by the CIMEL Sun photometer during the April 1994 RCS IOP. These radiometer-derived size distributions, integrated on the atmospheric column, are converted to true size distributions using an assumed aerosol scale height of 1.5 km [*Remer et al.*, 1997].

compared with the coincident lidar measurements. Since the Raman lidar measures both aerosol extinction and backscattering as functions of altitude, this technique has the advantage of being able to determine how real refractive index and single-scattering albedo vary with altitude. The disadvantage of this technique is that the derived single-scattering albedo is sensitive to the manner in which absorbing particles are represented in the aerosol mixture. The technique used here assumes the absorbing particles are much smaller than the wavelength and exist as distinct particles (external mixture).

This technique is applied to lidar and aerosol size distribution measurements acquired over the SGP site on the nights of April 21 and 24, 1994. The results show that the change in aerosol particle size with relative humidity as measured by this optical particle counter can be represented in the form discussed by *Hanel* [1976] with the exponent $\gamma = 0.3 \pm 0.05$. The real refractive

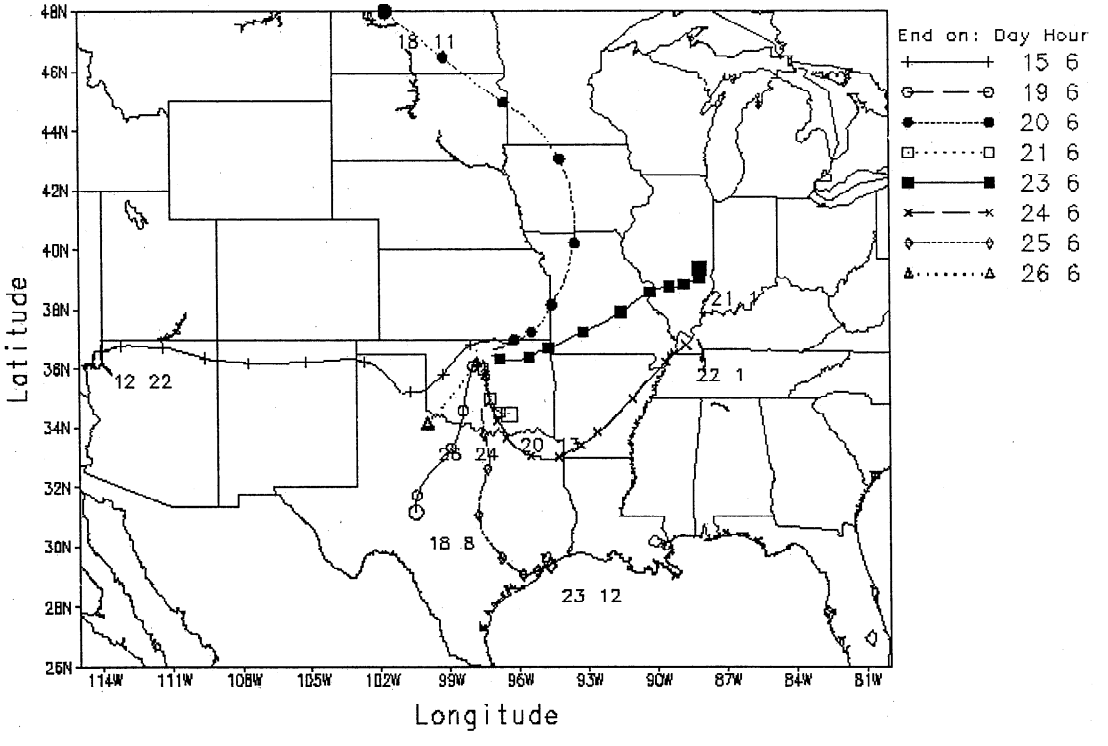

Figure 14. Three day back surface trajectories computed using the HYSPLIT3 trajectory model for selected days during the 1994 RCS IOP. Trajectories that end at the surface over the SGP at 0600 UT for April 15, 19, 20, 21, 23, 24, 25, and 26 are shown. The labels on each trajectory show the beginning day and time.

indices derived from these measurements were found to vary between 1.4–1.5 (dry) and 1.37–1.47 (wet). Uncertainties in the real refractive indices are ±0.05. Measurements acquired on April 21, 1994, showed the real refractive index decreased with altitude. The derived single-scattering albedos are generally found to be above 0.94 ± 0.1. However, on this same night, ω_0 decreased from 0.94 to 0.82 as the aerosol extinction and backscattering increased within the lower 1.4 km. In addition, a value of $\omega_0 = 0.7 \pm 0.1$ is derived for an elevated aerosol layer observed on this same night. This technique could be evaluated in future experiments by using in situ measurements of the aerosol composition and absorption to also estimate refractive index and single-scattering albedo. Since this SRL can scan and measure aerosols close to the surface, these additional measurements could be acquired at or near the surface and so would not necessarily require aircraft support.

Acknowledgements. The University of North Dakota Citation Aircraft involvement in the RCS IOP was funded by DOE under subcontract with the University of Utah (K. Sassen), contract 83221.

References

Ackerman, T., and O.B. Toon, Absorption of visible radiation in atmosphere containing mixtures of absorbing and nonabsorbing particles, *Appl. Opt.*, *20*(20), 3661–3667, 1981.

Baumgardner, D. and B. Huebert, The airborne aerosol inlet workshop: Meeting report, *J. Aerosol Sci.*, *24*(6), 835–846, 1993.

Bohren, C.F., and D.R. Huffman, *Absorption and Scattering of Light by Small Particles*, John Wiley, New York, 1983.

Brock, C. A., L. F. Radke, and P.V. Hobbs, Sulfur in particles in arctic hazes derived from airborne in situ and lidar measurements, *J. Geophys. Res.*, *95*, 22,369-22,387, 1990.

Charlson, R.J., D.S. Covert, and T.V. Larson, Observation of the effect of humidity on light scattering by aerosols, in *Hygroscopic Aerosols*, edited by L. Ruhnke and A. Deepak, pp. 35–44, A. Deepak, Hampton, Va., 1984.

Charlson, R.J., S.E. Schwartz, J.M. Hales, R.D. Cess, J.A. Coakley Jr., J.E. Hansen, and D.J. Hofmann, Climate forcing by anthropogenic aerosols, *Science*, *255*, 423–430, 1992.

d'Almeida, G.A., P. Koepke, and E.P. Shettle, *Atmospheric Aerosols: Global Climatology and Radiative Characteristics*, A. Deepak, 559 pp., Hampton, Va., 1991.

de Leeuw, G., G.J. Kunz, and C.W. Lamberts, Humidity effects on the backscatter/extinction ratio, *Appl. Opt.*, *25*(22), 3971–3973, 1986.

Draxler, R.R., *Hybrid Single-Particle Langrangian Integrated Trajectories (HY-SPLIT): Model Description, NOAA Tech. Memo., ERL ARL-166*, Natl. Oceanic and Atmos. Admin., Washington, D. C., 1988.

Fenn, R.W., E.P. Shettle, W.S. Hering, and R.W. Johnson, Atmospheric optical properties and meteorological conditions, *Atmos. Environ.*, *15*(10/11), 1911–1918, 1981.

Ferrare, R.A., S.H. Melfi, D.N. Whiteman, K.D. Evans, and R. Leifer, Raman lidar measurements of aerosol extinction and backscattering 1. Methods and comparisons, *J. Geophys. Res.*, this issue.

Fraser, R.S., and Y.J. Kaufman, The relative importance of aerosol scattering and absorption in remote sensing, *IEEE Trans. on Geoscio. Remote Sens.*, *23*, 625–633, 1985.

Fraser, R.S., R.A. Ferrare, Y.J. Kaufman, B.L. Markham, and S. Mattoo, Algorithm for atmospheric corrections of aircraft and satellite imagery, *Int. J. Remote Sens.*, *13*(3), 541–557, 1992.

Hanel, G., An attempt to interpret the humidity dependencies of the aerosol extinction and scattering coefficients, *Atmos. Environ.*, *15*, 403–406, 1976.

Hanel, G., The physical chemistry of atmospheric particles, in *Hygroscopic Aerosols*, edited by L. Ruhnke and A. Deepak, pp. 1–20, A. Deepak, Hampton, Va., 1984.

Hansen, J., M. Sato, and R. Ruedy, Radiative forcing and climate response, *J. Geophys. Res.*, *102*, 6831–6864, 1997.

Heintzenberg, J., R.J. Charlson, A.D. Clarke, C. Liousse, V. Ramaswamy, K.P. Shine, M. Wendisch, and G. Helas, Measurements and modelling of aerosol single-scattering albedo: Progress, problems, and prospects, *Contrib. Atmos. Phys.*, *70*, 249–263, 1997.

Huebert, B.J., G. Lee, and W.L. Warren, Airborne aerosol inlet passing efficiency measurement, *J. Geophys. Res.*, *95*, 16,369–16,381, 1990.

Intergovernmental Panel on Climate Change (IPCC), *Climate Change: Radiative Forcing of Climate Change: The Scientific Assessment*, 339 pp., Cambridge Univ. Press, New York, 1994.

Intergovernmental Panel on Climate Change (IPCC), *Climate Change, 1995: The Science of Climate Change*, 572 pp., Cambridge Univ. Press, New York, 1995.

Junge, C.E., *Air Chemistry and Radioactivity*, 382 pp., Academic, San Diego, Calif., 1963.

Kaufman, Y.J. and R.S. Fraser, Light extinction by aerosols during summer air pollution, *J. Clim. Appl. Meteorol.*, *22*, 1694–1706, 1983.

Kaufman, Y.J., A. Gitelson, A. Karnieli, E. Ganor, R.S. Fraser, T. Nakajima, S. Mattoo, and B.N. Holben, Size distribution and scattering phase function of aerosol particles retrieved from sky brightness measurements, *J. Geophys. Res.*, *99*, 10,341–10,356, 1994.

Kiehl, J.T., and B.P. Briegleb, The relative roles of sulfate aerosols and greenhouse gases in climate forcing, *Science*, *260*, 311–314, 1993.

King, M.D., D.M. Byrne, B.M. Herman, and J.A. Reagan, Aerosol size distribution obtained by inversion of optical depth measurements, *J. Atmos. Sci.*, *35*, 2153–2167, 1978.

Koepke, P. and M. Hess, Scattering functions of tropospheric aerosols: The effect of nonspherical particles, *Appl. Opt.*, *27*, 2422–2430, 1988.

Malm, W.C., J.V. Molenar, R.A. Eldred, and J.F. Sisler, Examining the relationship among atmospheric aerosols and light scattering and extinction in the Grand Canyon area, *J. Geophys. Res.*, *101*, 19,251–19,265, 1996.

McMurray, P.H., and M.R. Stolzenburg, On the sensitivity of particle size to relative humidity for Los Angeles aerosols, *Atmos. Environ.*, *23*, 497–507, 1989.

Mishchenko, M.I., A.A. Lacis, B.E. Carlson, and L.D. Travis, Nonsphericity of dust-like tropospheric aerosols: Implications for aerosol remote sensing and climate modeling, *Geophys. Res. Lett.*, *22*, 1077–1080, 1995.

Nakajima, T., M. Tanaka, and T. Yamauchi, Retrieval of the optical properties of aerosols from aureole and extinction data, *Appl. Opt.*, *22*, 2951–2959, 1983.

Nakajima, T., T. Takamura, M. Yamano, M. Shiobara, T. Yamauchi, R. Goto, and K. Murai, Consistency of aerosol size distribution inferred from measurements of solar radiation and aureole, *J. Meteorol. Soc. Jpn.*, *64*, 765–776, 1986.

Nilsson, B., Meteorological influence on aerosol extinction in the 0.2-40 mm wavelength range, *Appl. Opt.*, *18*(20), 3457–3473, 1979.

Nilsson, B., A. Hagard, and H. Ottersten, Investigation of the meteorological influence on aerosol transmission in the 0.5 mm to 14 mm wavelength range, in *Atmospheric Aerosols: Their Formation, Optical Properties, and Effects*, pp. 317–334, Spectrum Press, Hampton, Va., 1982.

Nizich, S.V., T. Pierce, W. Hohenstein, and E.H. Pechan, National Air Pollutant Emission Trends, 1900-1994, *EPA Rep. EPA-454/R-95-011*, Environ. Prot. Agency, Research Park Triangle, N.C., 1995.

Patterson, E.M., and G. Grams, Determination of aerosol absorption and scattering in the free troposphere, IRS'84, in Proceedings of the International Radiation Symposium on Current Problems in Atmospheric Radiation, pp. 29–31, A. Deepak, Hampton, Va. 1984.

Reagan, J.A., D.M. Byrne, M.D. King, J.D. Spinhirne, and B.M. Herman, Determination of the complex refractive index of atmospheric particulates from bistatic-monostatic lidar and solar radiometer measurements, *J. Geophys. Res.*, *85*, 1591–1599, 1980.

Remer, L., S. Gasso, D. Hegg, Y. Kaufman, and B. Holben, Urban/industrial aerosol: Ground-based Sun/sky radiometer and airborne in situ measurements, *J. Geophys. Res.*, *102*, 16,849–16,859, 1997.

Rood, M.J., T.V. Larson, D.S. Covert, and N.C. Ahlquist, Measurement of laboratory and ambient aerosols with temperature and humidity controlled nephelometry, *Atmos. Environ.*, *19*, 1181–1190, 1985.

Rosen, J.M., B.A. Bodhaine, J.F. Boatman, J.J. DeLuisi, M.J. Post, Y. Kim, R. C. Schnell, P.J. Sheridan, and D.M. Garvey, Measured and calculated optical property profiles in the mixed layer and free troposphere, *J. Geophys. Res.*, *97*, 12,837–12,850, 1992.

Shettle, E.P., and R.W. Fenn, Models for the aerosols of the lower atmosphere and the effects of humidity variations on their optical properties, *AFGL-TR-79-0214*, Air Force Geophys. Lab., Hanscom Air Force Base, Mass., 1979.

Shiobara, M. T. Hayasaka, T. Nakajima, and M. Tanaka, Aerosol monitoring using a scanning spectral radiometer in Sendai, Japan, *J. Meteorol. Soc. Jpn.*, *69*, 57–70, 1991.

Sloane, C.S., Effect of composition on aerosol light scattering efficiencies, *Atmos. Environ.*, *20*(5), 1025–1037, 1986.

Sloane, C.S., and G.T. Wolff, Prediction of ambient light scattering using a physical model responsive to relative humidity: Validation with measurements from Detroit, *Atmos. Environ.*, *19*(4), 669–680, 1985.

Strapp, J.W., W.R. Leaitch, and P.S.K. Liu, Hydrated and dried aerosol-size-distribution measurements from the particle measuring systems FSSP-300 probe and the deiced PCASP-100X probe, *J. Atmos. Oceanic Technol.*, *9*, 548–555, 1992.

Svenningsson, I.B., H.C. Hansson, and A. Wiedensohler, Hygroscopic growth of aerosol particles in the Po Valley, *Tellus*, *Ser. B.*, *42*, 556–569, 1992.

Takamura, T., and Y. Sasano, Ratio of aerosol backscatter to extinction coefficients as determined from angular scattering measurements for use in atmospheric lidar applications, *Opt. Quant. Electron.*, *19*, 293–302, 1987.

Takamura, T., and Y. Sasano, Aerosol optical properties inferred from simultaneous lidar, aerosol-counter, and Sun photometer measurements, *J. Meteorol. Soc. Jpn.*, *68*(6), 729–739, 1990.

Takamura, T., Y. Sasano, and T. Hayasaka, Tropospheric aerosol optical properties derived from lidar, Sun photometer, and optical particle counter measurements, *Appl. Opt.*, *33*(30), 7132–7140, 1994.

Tang, I.N., Phase transformation and growth of aerosol particles composed of mixed salts, *J. Aerosol Sci.*, *7*, 361–371, 1976.

Tang, I.N., H.R. Munkelwitz, and J.G. Davis, Aerosol growth studies, IV, Phase transformation of mixed salt aerosols in a moist environment, *J. Aerosol Sci.*, *9*, 505–511, 1978.

Twomey, S. The influence of pollution on the short wave albedo of clouds, *J. Atmos. Sci.*, *34*, 1149–1152, 1977.

Twomey, S., Aerosols, clouds, and radiation, *Atmos. Environ.*, *25*, *Ser. A.*, 2435–2442, 1991.

van de Hulst, H.C., *Light Scattering by Small Particles*, 470 pp., John Wiley, New York, 1957.

von Hoyningen-Huene, W., and M. Wendisch, Variability of aerosol optical parameters by advective processes, *Atmos. Environ.*, *28*, 923–933, 1994.

Wendisch, M., and W. von Hoyningen-Huene, Optically equivalent refractive index of atmospheric aerosol particles, *Contr. Atmos. Phys.*, *65*, 293–309, 1992.

R.A. Ferrare, NASA Langley Research Center, Mail Stop 401A, Bldg. 1250, Room 132A, 21 Langley Blvd., Hampton, VA 23681 (e-mail: r.ferrare@larc.nasa.gov)

S.H. Melfi, Dept. of Physics, University of Maryland Baltimore County, Baltimore, MD 21250.

Y.J. Kaufman, D.N. Whiteman, NASA Goddard Space Flight Center, Greenbelt, MD 20771.

K.D. Evans, Joint Center for Earth Systems Technology, University of Maryland Baltimore County, Baltimore, MD 21250.

M. Poellot, Dept. of Atmospheric Sciences, University of North Dakota, Grand Forks, ND 58202.

(Received December 27, 1997; revised April 13, 1998;
accepted May 5, 1998.)